

Deep Roto-Translation Scattering for Object Classification

Edouard Oyallon and Stéphane Mallat
Département Informatique, ENS
45 rue d'Ulm, 75005 Paris
edouard.oyallon@ens.fr

Abstract

Dictionary learning algorithms or supervised deep convolution networks have considerably improved the efficiency of predefined feature representations such as SIFT. We introduce a deep scattering convolution network, with predefined wavelet filters over spatial and angular variables. This representation brings an important improvement to results previously obtained with predefined features over object image databases such as Caltech and CIFAR. The resulting accuracy is comparable to results obtained with unsupervised deep learning and dictionary based representations. This shows that refining image representations by using geometric priors is a promising direction to improve image classification and its understanding.

1. Introduction

Learning image representations has considerably enhanced image classification results compared to geometric features such as edge descriptors, or, SIFT and HOG [17, 5] patch representations. Learning may thus seem to be a more promising direction for improving image analysis rather than refining geometric image analysis. This paper aims at showing that understanding how to take advantage of geometrical image properties can define image representations, providing competitive results with state of the art unsupervised learning algorithms. It shows that refining geometric image understanding remains highly promising for image classification. We also provide a mathematical and algorithmic framework for doing so.

Supervised deep neural network learning achieves state-of-the-art results on many databases [9, 14]. However, several works [30, 6] have shown that the Alex-net [9] trained on ImageNet still performs very well on different databases such as Caltech or PASCAL VOC. The output of this neural network can thus be considered as a “super SIFT” image descriptor, which is used as an input to a linear SVM classifier [30, 6]. It indicates that this deep network is capturing important generic image properties, which are not

dependent upon the classes used for training. In the same spirit, unsupervised deep learning [11] as well as unsupervised bag of words [26] or dictionary learning with spatial pyramid [10] have improved classification results previously obtained with engineered feature vectors such as SIFT or HOG, on complex object recognition databases. However, these unsupervised learning algorithms are tailored to each databases. One may wonder whether their improved performances result from an adaptation to the specific properties of each databases, or whether these unsupervised representations capture refined geometric image properties compared to SIFT or HOG features.

A scattering convolution network is constructed with predefined wavelet filters, which are adapted to geometric image variabilities [20]. It provides a mathematical and algorithmic framework to incorporate refined geometric image priors within the representation. Since images are projections of 3D scenes under various view points, the main source of geometric image variabilities comes from rigid movements, and deformations resulting from perspective projections. An important issue is to build adaptive invariants to these sources of variability, which preserve essential information to discriminate different classes. A translation invariant scattering network was studied in [4] for digit image classification and texture recognition, but which was not powerful enough to classify complex objects as in Caltech or CIFAR. A translation and rotation invariant deep scattering network was introduced in [25] to classify textures with strong rotations and scalings. However, imposing rotation invariance is a prior which is too strong for image object and scene classifications, which are typically not fully rotation invariant.

Section 2 introduces a scattering representation which is translation invariant, and which efficiently represents rotation variability without imposing full rotation invariance. It yields a representation which complements SIFT type coefficients, with coefficients incorporating interactions between scales and angles. This roto-translation scattering representation is nearly complete in the sense that good quality images can be recovered from roto-translation scat-

tering coefficients [3]. It is also stable to additive perturbations and small deformations, which guarantees to avoid the type of instability observed in some deep networks [28]. In this architecture, the loss of information only appears at the final supervised classification stage, which computes invariants adapted to the classification task. It includes a partial least square supervised feature selection followed by a linear or a Gaussian kernel SVM.

This scattering representation is tested in Section 4 over Caltech and CIFAR data bases for object classification. It yields results which are well above all other representation which do not incorporate any learning, based on SIFT type features or with random weight deep networks. It also yields competitive results with state of the art unsupervised learning procedure adapted to each databases, which indicates that these unsupervised learning algorithm do not capture geometric transformations which are more powerful than rigid movements and small deformations. Computations can be reproduced with a software that will be available on-line. Generic supervised learning networks such as Alex-net, trained on Imagenet provides better classification rates. The refined geometry captured by these networks is further discussed.

2. Roto-Translation Scattering Networks

Images have important geometric variability due to perspective projections of 3D scenes under various viewpoints. It includes a combination of rigid movements and deformations. This section introduces a separable scattering transform, which constructs a nearly complete representation, based on elementary features, which linearizes important geometric variability. This representation is used for object classification. Scattering networks are particular classes of convolution networks [20], whose filters are computed with wavelets. They are introduced in the framework of convolution networks to better understand the specificities of their architecture.

2.1. Convolution Network Cascade

A convolutional network is a multilayer architecture, which cascades spatial convolutions and pooling operators, which includes sub-samplings [13]. These networks compute progressively more invariant image descriptors over multiple layers indexed by $0 \leq j \leq J$.

For $j = 0$, the network illustrated in Figure 1 takes in input an image x of P pixels, with potentially $Q_0 = 3$ color frames. For $j > 0$, each layer $x_j(p, q)$ is a set of Q_j image frames, which correspond to different “feature types” indexed by $1 \leq q \leq Q_j$. Each feature image has P_j pixels indexed by p . It is computed from x_{j-1} by applying a linear operator F_j to x_{j-1} , followed by a non-linearity, which may be a rectifier, a thresholding, a modulus or some other non-linearities “pooling” functions [13]. Convolution networks

impose that for each fixed q , F_j computes a convolution of $x_{j-1}(p, q)$ along p , with a filter which depends upon q . The operator F_j also linearly combines the Q_{j-1} image frames of x_{j-1} indexed by q . The output vector $F_j x_{j-1}$ is then transformed by a non-linear “pooling operator” which may incorporate a rectifier, a modulus, a thresholding [13]. For scattering transforms, $F_j x_{j-1}$ is a complex valued signal and the non-linearity is a complex modulus, so we write:

$$x_j = |F_j| x_{j-1}. \quad (1)$$

Figure 1 illustrates this computational architecture introduced by LeCun [13].

The operators $|F_j|$ progressively propagate x across the network until the last layer x_J . The cascade of convolutions produce operators of progressively wider supports as j increase. The depth j thus corresponds to a scale index of the non-linear network features. A classifier is applied to the output x_J . It may be a linear SVM, a RBF network, or some other fully connected double layer classification networks [9, 13]. In our numerical experiments, we use a dimensionality reduction step followed by a Gaussian SVM.

The network architecture is specified by the dimensions $P_j \times Q_j$ of each layer and by the non-linear pooling operator. This is a delicate step, which is usually done through an ad-hoc engineering trial and error process. Given this architecture, one must then optimize each operators F_j to achieve a low classification error. Experiments have been performed with random weights [23]. Better results are however obtained with unsupervised training of the weights, using auto-encoders [29]. When enough labeled examples are available, even better results are obtained with supervised training algorithms which back-propagates classification errors [12]. The Alex-Net is an example of supervised deep network trained with labeled images of the ImageNet data basis [9].

2.2. Scattering Network

A scattering network is a convolutional network whose architecture and filters are not learned, but are predefined wavelets. These wavelets are adapted to the type of geometric invariants and linearization that need to be computed. Image classification typically requires to build image features which are locally invariant to translations and stable to deformations. It should thus linearize small deformations so that these deformations can be taken into account or removed with a linear operator, which is adjusted by the final supervised classifier.

Scattering networks compute inner-layer coefficients $x_j(p, q)$, which are nearly invariant to translations of the input image x by less than 2^j . Each image frame is sub-sampled at intervals 2^{j-1} . The factor 2 oversampling avoids aliasing phenomena. If x has P pixels then each network layer x_j has Q_j frames of $P_j = P 2^{-2j+2}$ pixels. The

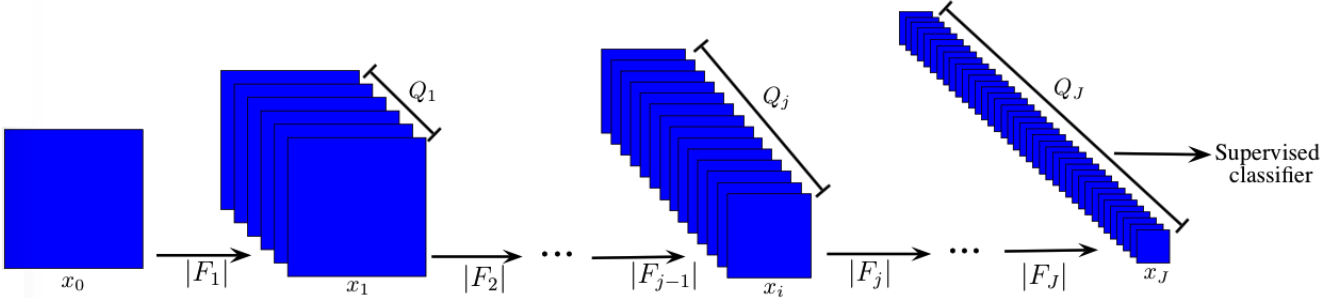


Figure 1. A convolution network computes a layer x_j by applying a linear operator F_j to x_{j-1} , followed by a non-linearity which we choose to be a modulus.

size Q_j does not result from an ad-hoc decision but depends upon the choice of geometric invariant as we shall see.

It has been proved mathematically that translation invariance and linearization of deformations is obtained with wavelets [20]. They separate the image information along multiple scales and orientations. Cascading wavelet transforms and modulus non-linearities lead to translation invariant scattering transforms [20], which have been applied to digit and texture classifications [4]. Rotation invariant scattering networks have been introduced by replacing wavelet spatial convolutions by convolutions along the special Euclidean group of rigid movements. It takes into account both translations and rotations [25]. We introduce a simpler separable convolution, which still has the ability to build invariants over rigid movements, but which leaves the choice of invariant to the final SVM classifier.

Wavelet transforms can be computed with a cascade of linear filtering and sub-sampling operators, which are called multi-rate filter banks [19]. Although deep networks apply non-linearities at each layer, they have such linear cascades because rectifier or modulus non-linearities have no impact over positive coefficients produced by averaging filters in the network. All non-linearities can thus be removed from averaging filters output. Deep network computations can therefore be factorized as a cascade of $j_1 - 1$ averaging and sub-sampling operators, followed by a band-pass filter and a non-linearity, followed again by a cascade of $j_2 - 1$ averaging operators, followed by a band-pass filter and a non-linearity, and so on. If the network includes a sub-sampling by a factor 2 at each layer, then this is equivalent to a convolution with a wavelet of scale 2^{j_1} followed by a non-linearity, followed by a second convolution with a wavelet of scale 2^{j_2} and a second non-linearity, and so on. The scales depend upon the number of averaging and sub-samplings along each network path, and thus satisfy $1 \leq j_1 < j_2 \leq J$.

In the following, we describe a second order scattering transform operator S_J , which performs at most two wavelet convolutions. The network output x_J is computed with a first $2D$ spatial wavelet transform W_1 which per-

forms spatial wavelet image convolutions whose phase are removed by a non-linear modulus. We then apply a second wavelet transform W_2 , which is adapted to the desired invariants, not only along translations but also along rotations. This is done by computing separable $2D$ convolutions with wavelets along space, and $1D$ convolutions with wavelet along angle variables. The output is averaged by an operator A_J which performs a spatial averaging at the scale 2^J :

$$x_J = S_J x = A_J |W_2| |W_1| x .$$

Higher order scattering transforms are obtained by cascading more wavelet transforms, which can be adapted to other group of transformations. However, this paper concentrates on second order scattering along space and rotation variable. This second order should not be confused with the network depth J , which corresponds to the maximum spatial invariance scale 2^J , and typically depends upon the image size. Next two sections describe the implementations of the two wavelet transforms W_1 and W_2 and the averaging operator A_J .

2.3. Spatial Wavelet Transform W_1

The first wavelet transform W_1 separates the image component along different scales and orientations, by filtering the image x with a family of wavelet $\psi_{j,\theta}$. These wavelets are obtained by dilating by 2^j a mother wavelet $\psi(p)$, and rotating its support with r_θ along L angles θ :

$$\psi_{j,\theta}(p) = 2^{-2j} \psi(2^{-j} r_\theta p) \text{ for } \theta = \frac{l\pi}{L} .$$

As in [4, 25], we choose a complex Morlet wavelet ψ derived from a Gaussian modulated by a complex exponential. Figure 2 shows the real and imaginary parts of Morlet wavelets along $L = 8$ angles. The modulus computes the envelop of complex wavelet coefficients, sub-sampled at intervals 2^{j-1} . Coefficients at the scale 2^j are stored at the depth j :

$$x_j^1(p, \theta) = |x \star \psi_{j,\theta}(2^{j-1} p)| .$$

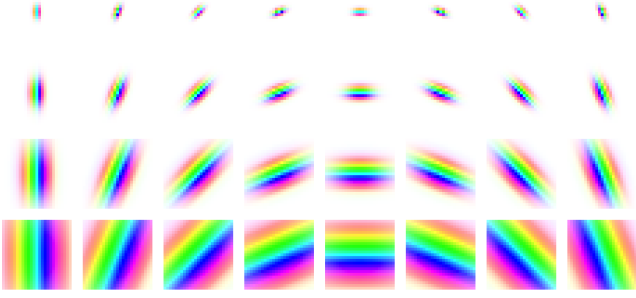


Figure 2. Real and imaginary parts of Morlet wavelets at different scales 2^j for $1 \leq j \leq 4$ and $L = 8$ orientations. Phase and amplitude are respectively given by the color and the contrast.(best viewed in color)

These coefficients are nearly invariant to a translation of x smaller than 2^j . For $2^j < 2^J$, this invariance will be improved by further propagating these coefficients up to layer J , with a second wavelet transform described in the next section.

Coefficients at the scale 2^j correspond to deep network coefficients of depth j because in a deep network they are calculated by cascading $j - 1$ low-pass filters, and a final band-pass filter. The cascade of low-pass filters defines a pyramid of low-passed images $x \star \phi_j$, where ϕ_j is a scaled low-pass filter:

$$\phi_j(p) = 2^{-2j} \phi(2^{-j}p).$$

Each $x \star \phi_j$ is computed by convolving $x \star \phi_{j-1}$ with a low-pass filter h followed by a sub-sampling. It is stored as an image indexed by $q = 0$ in the layer j :

$$x_j^1(p, 0) = x \star \phi_j(p) = h \star (x \star \phi_{j-1})(2p). \quad (2)$$

Applying a modulus has no effect because these coefficients are positive. The wavelet coefficients $x \star \psi_{j,\theta}$ are computed by applying a complex band-pass filter g_θ followed by a sub-sampling. In this case, the modulus has a strong impact by eliminating the complex phase. It is stored as an image indexed by $q = \theta$ in the layer j :

$$x_j^1(p, \theta) = |x \star \psi_{j,\theta}(p)| = |g_\theta \star (x \star \phi_{j-1})(p)|. \quad (3)$$

The wavelet transform W_1 is thus implemented in a deep network calculated with a cascade of low-pass and band-pass filtering, followed by sub-samplings, illustrated in Figure 3. Wavelet coefficients are computed at scales $2^j \leq 2^J$ and the lowest frequency image information is carried by the remaining averaged image $x \star \phi_J$. The convolution cascades (2) and (3) with h and g_θ can also be computed directly as convolutions with ϕ_j and $\psi_{j,\theta}$, using FFT's. For the sake of simplicity, we follow this second approach and thus specify directly the ϕ and ψ as opposed to the intermediate filters h and g_θ . We use a Morlet wavelet ψ and

a Gaussian filter ϕ , further specified in [4]. The resulting wavelet transform W_1 is a contractive linear operator, which is nearly an isometry.

2.4. Roto-Translation Wavelet Transform W_2

Wavelet coefficients $|x \star \psi_{j,\theta}|$ are translation invariant only up to the scale 2^j . Increasing this invariance up to 2^J means further propagating these coefficients up to the last network layer J . This is done by applying a second wavelet transform W_2 which is now defined. This second wavelet transform also recombines the output of wavelet filters along different angles. It thus also measures the angular variability of wavelet responses, as corner detectors.

At a depth j_1 , there are $\tilde{Q}_{j_1} = L$ wavelet image frames indexed by the angle $\theta_1 = l\pi/L$ for $1 \leq l \leq L$:

$$x_{j_1}^1(p, \theta) = |x \star \psi_{j_1, \theta_1}(2^{j_1-1}p)|.$$

These coefficients are propagated to larger scales 2^j by computing convolutions and modulus with a new set of spatial wavelets $\psi_{j,\theta}(p)$ at larger scales $2^j > 2^{j_1}$.

As in deep convolution network architectures, we also recombine the information in these image frames indexed by the angle θ in (3). To understand how to do so, let us look at the impact on wavelet coefficients of a rotation r_α of $x(\cdot)$ by an angle α :

$$x(r_\alpha \cdot) \star \psi_{j_1, \theta_1}(p) = x \star \psi_{j_1, \theta_1 - \alpha}(r_\alpha p).$$

Besides a rotation of spatial coordinates, it “translates” the angle parameter θ_1 by α .

Our goal is not to build a rotation invariant representation but a representation which linearizes large rotations. Rotation variabilities can thus be discriminated or removed by a linear classifiers at the output. We thus do not use a rotation invariant scattering representation as in [25]. To build a representation which is stable to rotations and deformations along rotations, we compute a wavelet transform along the angle parameter θ_1 , which means performing convolutions along θ_1 , with wavelets $\psi_l(\theta_1) = 2^{-l} \psi(2^{-l}\theta_1)$. The resulting wavelet transform W_2 computes separable convolutions along both the $2D$ spatial variable p and the angle variable θ_1 , with a $3D$ separable complex wavelet defined by:

$$\psi_{j,\theta,k}(p, \theta_1) = \psi_{j,\theta}(p) \psi_k(\theta_1).$$

It is a separable product of a spatial wavelet $\psi_{j,\theta}(p)$ of scale 2^j and an angular wavelet $\psi_k(\theta_1)$ of scale 2^k for $1 \leq k \leq K < \log_2 L$. If $\psi_k(\theta_1)$ are one-dimensional Morlet wavelets, then the resulting separable wavelet transform W_2 is a stable and invertible operator, which nearly preserves the signal norm.

The wavelet transform modulus for $j > j_1$ is computed with a three-dimensional separable convolution along

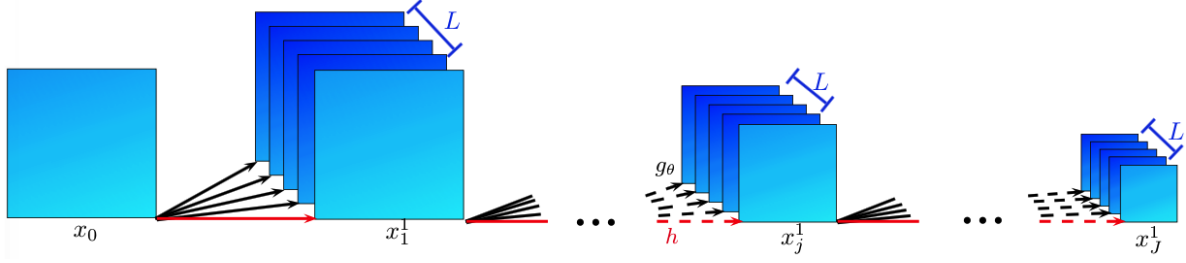


Figure 3. A wavelet modulus $|W_1|$ computes averages and modulus wavelet image frames at each layer x_j^1 , by cascading filtering, subsampling and modulus operators.

the spatial and angular variables, and it performs a subsampling along both variables. It has a spatial scale 2^j and is thus stored at the layer j via an index q which encodes θ , j_1 and k :

$$x_j^2(p, q) = |x_{j_1}^1 \star \psi_{j, \theta, k}(2^{-j-1}p)|. \quad (4)$$

It propagates $x_{j_1}^1$ towards network layers of depth $j > j_1$, up to $j = J$. This 3D separable wavelet transform is either computed with a cascade of filtering across the deep network layers, or directly with 3D convolutions calculated with *FFT's*.

For $j < J$, we still need to propagate the second order coefficients x_j^2 up to the largest spatial scale 2^J . This could be done by applying a third wavelet transform W_3 which could also enforce more complex geometric invariants by recombining information across angles and scales. In this implementation, we directly apply a linear averaging $x_j^2 \star \phi_J$ at the scale 2^J . It averages each image frame of x_j^2 with a spatial convolution with $\phi_J(p) = 2^{-2J} \phi(2^{-J}p)$.

The last layer x_J of this scattering network is an aggregation of the image x , of first order wavelet modulus images x_j^1 , and of second order coefficients x_j^2 at all scales $2^j \leq 2^J$, all of them averaged at the scale 2^J :

$$x_J = S_J x = \left\{ x \star \phi_J, x_j^1 \star \phi_J, x_j^2 \star \phi_J \right\}_{1 \leq j \leq J}.$$

First order coefficients $x_j^1 \star \phi_J$ are very similar to SIFT [17] feature vectors. They provide information on average energy distributions across scales and orientations over a neighborhood of size 2^J . A scattering representations can thus be interpreted as an ‘‘augmented’’ SIFT representation with second order coefficients $x_j^2 \star \phi_J$ providing information on interactions between scales and angles in multi-scale neighborhoods.

This deep scattering cascade is thus the product of the modulus $|W_1|$ of a first 2D spatial wavelet transform, followed by the modulus $|W_2|$ of a second 3D separable wavelet transform along space and angles, followed by the averaging $A_J z = z \star \phi_J$:

$$S_J x = A_J |W_2| |W_1| x.$$

Since W_1 and W_2 and A_J are contractive operators it guarantees that S_J is also contractive and hence stable to additive perturbations. Moreover, since the wavelet transforms W_1 and W_2 and A_J are Lipschitz stable relatively to deformations [20], S_J is also Lipschitz and hence linearizes small deformations. This guaranties to avoid the instabilities observed on deep networks such as Alex-net [28] where a small image perturbation can considerably modify the network output and hence the classification.

For images of P pixels, each network layer x_j has Q_j image frames of $P_j = P 2^{-2j+2}$ pixels. For a gray level image such that $Q_0 = 1$, the resulting number of frames are respectively $Q_1 = 9$, $Q_2 = 81$, $Q_3 = 217$, $Q_4 = 417$, $Q_5 = 681$, $Q_6 = 1009$, and $Q_j \approx 64j^2$ when $j \gg 1$. Color images are represented by the three Y,U,V color bands, and each color band is decomposed independently. It thus multiplies the number of image frames Q_j by 3 for all $0 \leq j \leq J$. It has been shown that as long as there are as much scattering coefficients as the number of pixels in the original image, one can reconstruct images of good quality from the scattering representation [3]. It means that despite the invariance to translation, the roto-translation scattering representation is nearly complete.

3. Supervised Feature Selection

The scattering representation has a number of coefficients which is of the same order as the original image. It provides a nearly complete signal representation, which allows one to build a very rich set of geometric invariants with linear projection operators. The choice of these linear projection operators is done at the supervised classification stage with a SVM. Results are however improved by a first supervised feature selection, which applies a linear operator to reduce the number of scattering coefficients and decorrelate them, before computing an SVM classifier. The feature selection is implemented with a partial least square regression [22, 31, 24].

A logarithm non-linearity is applied to scattering coefficients in order to separate low frequency multiplicative components due to the variations of illuminations. These low-frequency modulations add a constant to the logarithm

of scattering coefficients which can then be removed with an appropriate linear projector by the final classifier. Also, it linearizes exponential decay of the scattering coefficients across scales.

In the following, we denote by $\Phi x = \{\phi_p x\}_p$ the centered logarithm of scattering coefficients at a scale 2^J . We perform a feature selection adapted to each class C , with a partial least square regression of the one-versus-all indicator function

$$f_C(x) = \begin{cases} 1 & \text{if } x \text{ belongs to class } C \\ 0 & \text{otherwise} \end{cases}.$$

A partial least square greedily selects and orthogonalizes each feature, one at a time. At the k^{th} iteration, it selects a $\phi_{p_k} x$, and a Gram-Schmidt orthogonalization yields a normalized log scattering feature $\tilde{\phi}_{p_k} x$, which is uncorrelated relatively to all previously selected features:

$$\forall r < k, \sum_i \tilde{\phi}_{p_k}(x_i) \tilde{\phi}_{p_r}(x_i) = 0 \text{ and } \sum_i |\tilde{\phi}_{p_k}(x_i)|^2 = 1.$$

The k^{th} feature $\phi_{p_k} x$ is selected so that the linear regression of $f_C(x)$ on $\{\tilde{\phi}_{p_r} x\}_{1 \leq r \leq k}$ has a minimum mean-square error, computed on the training set. This is equivalent to finding ϕ_{p_k} which maximizes the correlation $\sum_i f_C(x_i) \tilde{\phi}_{p_k}(x_i)$.

The partial least square regression thus selects and computes K scattering features $\{\phi_{p_k} x\}_{k < K}$ for each class C , which are linearly transformed into K decorrelated and normalized features $\{\tilde{\phi}_{p_k} x\}_{k < K}$. For a total of n_C classes, the union of all these feature defines a dictionary of size $M = K n_C$. They are linear combinations of the original log scattering coefficients $\{\phi_p x\}_p$. This dimension reduction can thus be interpreted as a last fully connected network layer, which outputs a vector of size M . The parameter M governs the bias versus variance trade-off. It can be adjusted from the decay of the regression error of each f_C [22] or fixed a priori.

The improvement provided by the feature reduction is illustrated on the CIFAR-10 data basis by comparing the performance of a K-nearest neighbor classifier before and after dimensionality reduction. For CIFAR-10, the input scattering vector is of size $2 \cdot 10^4$. A K-nearest neighbor classifier as an accuracy of 55% before dimension reduction, for $K = 10$. This accuracy increases to 70% by reducing the dimension to $M = 1500$, with the partial least square selection.

Better classification results are however obtained by using SVM classifiers rather than K-nearest neighbor. The dimension reduction provides a less dramatic improvements but allows to slightly localize the linear classification by using a Gaussian kernel. The variance of this Gaussian kernel is set to the average norm of the scattering vectors, calculated from the training set. This large variance produces a

relatively small localization in the feature space, but it reduces classification errors by 3 – 5% on most databases. This Gaussian kernel classification can be considered as a coarsely localized linear classifier in this context.

4. Image Classification Results

We compare the performance of a scattering network with state-of-the-art algorithms on CIFAR and Caltech datasets, which include complex object classes.

Images of each databases are rescaled to become square images of 2^{2d} pixels. The scattering transform depends upon few parameters which are fixed a priori. The maximum scale of the scattering transform is set to $2^J = 2^{d-2}$. Scattering coefficients are thus averaged over spatial domains covering 1/4 of the image width, and coefficients sampled over a spatial grid of 4×4 points, a final down-sampling being performed without degrading classification accuracies. This preserves some coarse localization information. Coefficients are computed with Morlet wavelets having $L = 8$ orientations. The wavelet transform along these $L = 8$ angles are computed at a maximum scale $2^K = L/2$, which corresponds to a maximum angular variation of $\pi/2$. Indeed these object recognition problems do not involve larger rotation variability. The resulting scattering representation is nearly complete as previously explained. It is computed independently along the 3 color channels YUV. We apply a logarithm to separate illumination components. The classifier is implemented by first reducing the dimensionality, to $M = 1500$ feature vectors on CIFAR-10 for instance, with a partial least square regression, followed by a Gaussian kernel classifier.

Caltech-101 and Caltech-256 are two color image databases, with respectively 101 and 256 classes. They have 30 images per class for training and the rest is used for testing. Caltech images are rescaled to square images of $2^{2d} = 256^2$ pixels. Average per class classification results are reported with an averaging over 5 random splits. We removed the clutter class both from our training and testing set.

CIFAR are more challenging color image databases due to its high class variabilities, with 60000 tiny colors images of $2^{2d} = 32^2$ pixels. CIFAR-10 has 10 classes with 5000 training images per class, whereas CIFAR-100 has 100 classes with 500 training images per class.

The Tables 1,2,3,4 report the classification accuracy of different algorithms, organized in four broad categories. To normalize experiments, we only consider classifications performed without data augmentation. The ‘‘Prior’’ feature class applies a linear or an RBF type classifier to a set of features which are not computed from training data. Scattering, SIFT and HOG vectors, or deep networks with random weights belong to this Prior class. The ‘‘Unsup. Deep’’ category concerns unsupervised convolutional deep learn-

ing algorithms, whose filters are optimized with non-labeled training data, before applying a linear classifier or Gaussian kernel SVM. The “Unsup. Dict.” category includes one, two or three successive unsupervised sparse dictionary learning algorithms to SIFT type feature vectors or normalized pixel patches. It is often followed by a max-pooling operator over a pyramid structure [10]. The “Supervised” class corresponds to feature or kernel representations optimized with supervised learning over labeled training data. The training may be performed on a different databases such as ImageNet. It corresponds to supervised deep convolution networks or supervised kernel learning algorithms.

The scattering networks yield classification results which are well above results reported in Table 1,2,3,4 by all pipelines using prior features, which do not involve any learning, on Caltech-101 and CIFAR-10. A classification with SIFT features, without unsupervised dictionary learning, to which we apply a spatial pyramid pooling and a linear SVM classifier has an accuracy of 43% on Caltech-101. Applying a random matrix multiplication to SIFT features before pooling increases the accuracy to 50%. The substantial obtained improvement of scattering over SIFT is due to the second order coefficients. Indeed, first order are similar to SIFT descriptors [4], whereas the second order is discriminative along rotation and still builds invariance to translation. Also, [3] shows second order coefficients provide important joint information across scales and across angles. Convolutional network with random filters on mono-CIFAR-10 (gray level CIFAR-10) have an accuracy of 53.2% in [23]. When using color images as opposed to gray level images, the accuracy on CIFAR-10 improves by less than 10% for most algorithms, which remains below 83%. We did not find any result on the application of predefined “prior” features on CIFAR-100.

Table 1 and 3 shows that scattering networks performs at least as well as unsupervised deep convolutional architectures without data augmentation on Caltech-101 and CIFAR-10. It shows that unsupervised learning algorithms applied on deep networks capture representations that are at least as discriminative as the scattering representation. To our knowledge, no result with unsupervised deep convolutional network learning have been reported on Caltech-256.

State-of-the-art unsupervised classification results for Caltech, without data augmentation, are obtained with a Multipath-SC algorithm [1], which has 3 unsupervised encoding layers. Similar results are obtained with Spatial Local Coding descriptors [21] with a first layer of nearly SIFT descriptors followed by an unsupervised coding and multi-scale pyramidal pooling. Caltech-101 is an easier data basis because it has a bias across classes, which is typically used by classifiers. This bias is removed from Caltech 256 which explains why classifiers have a lower accuracy. The unsupervised classification algorithm reporting state of the

Method	Type	Accuracy
ScatNet	Prior	79.5
SIFT	Prior	42.4
Random Filters [13]	Prior	62.9
CDBN [15]	Unsup. Deep	65.4
M-HMP[1]	Unsup. Dict	82.5
SLC [21]	Unsup. Dict	81.0
Ask the locals [2]	Unsup. Dict	77.3
RFL [8]	Unsup. Dict	75.3
CNN [7]	Supervised	91.4

Table 1. Results for different types of representations on Caltech-101.

Method	Type	Accuracy
ScatNet	Prior	42.8
M-HMP [1]	Unsup. Dict	50.7
SLC [21]	Unsup. Dict	46.6
Ask the locals [2]	Unsup. Dict	41.7
CNN [30]	Supervised	70.6

Table 2. Results for different types of representations on Caltech-256.

Method	Type	Accuracy
ScatNet	Prior	82.2
RFL [8]	Unsup. Dict	83.1
NOMP [16]	Unsup. Dict	82.9
LIFT [27]	Unsup. Deep	82.2
CNN [14]	Supervised	91.8

Table 3. Results for different types of representations on CIFAR-10.

art results on CIFAR are different from the one on Caltech, which shows that these figures must be analyzed with precaution. Scattering method is comparable with all methods on both CIFAR-10 and CIFAR-100.

Let us emphasize that we are using the same scattering representation, besides the image size adaptation, for the Caltech and CIFAR databases. RFL [8] is an unsupervised learning algorithm which reports close to state of the art results, both on Caltech and CIFAR data bases. RFL does not perform as well as a scattering on Caltech and CIFAR-100, and slightly better on CIFAR-10. This illustrates the difficulty to have a single algorithm which works efficiently on very different databases. We reported the result on CIFAR-100 from [8] via [18].

State-of-the-art results are obtained by supervised deep convolutional network [14, 7, 30], that improves the non-supervised results by around 10% on CIFAR-10 or Caltech-101, 20% on Caltech-256, but 5% on CIFAR-100. The improvement on CIFAR-100 is smaller than on CIFAR-10

Method	Type	Accuracy
ScatNet	Prior	56.3
RFL [8]	Unsup. Dict	54.2
NOMP [16]	Unsup. Dict	60.8
CNN [14]	Supervised	65.4

Table 4. Results for different types of representations on CIFAR-100.

because there is only 500 samples per classes for supervised training, as opposed to 5000. The Caltech data bases does not have enough training sample to train a supervised deep network. We are thus reporting classification results obtained by the supervised Alex-network trained on ImageNet, to which is applied a linear SVM classifier which is trained on Caltech [6]. So, the issue of the lacks of samples does not occur for Caltech-256 since the supervised network has been pretrained on ImageNet. Although it is not trained on Caltech, it still achieves the state of the art on this databases. Experiments show that if the training and testing image datasets are different, a supervised deep network provides a feature vector having a lower accuracy for classification, but this accuracy is not dramatically reduced. It indicates that supervised deep classifiers are learning generic image representations which are likely to capture more complex geometric properties than unsupervised algorithms or a roto-translation scattering transform.

A scattering transform can be adapted to a group of operators acting on the image by defining wavelets convolutions on this group. In this paper we concentrate on translations, rotations and small deformations. We do not introduce any interaction with the color space since we apply separate transformations on each color band. Deep networks apply non-linear transformations across color bands. More complex groups could be considered, across color components, scaling, or subgroups of semi-direct products of translation rotation and scaling groups. The action of such groups can be linearized by defining wavelet transforms on the corresponding group. We know mathematically and algorithmically how to compute wavelet transforms on large classes of Lie groups or finite groups [20]. One can thus define a scattering transform on these groups. However, the main difficulty is to understand which groups play an important role in image classification problems. It seems that supervised classifiers have the ability to identify these finer transformations which could explain their improved performances.

5. Conclusion

This work shows that feature vectors for image classification can be constructed from geometric image properties as opposed to learning. A roto-translation scattering transform constructs a feature vector providing joint infor-

mation along multiple scales and multiple angles. For complex object classification problems as in Caltech and CIFAR databases, it considerably improves the performance of all existing prior image descriptors, and it yields comparable results with state of the art unsupervised deep learning, and dictionary learning algorithms.

Scattering networks are guaranteed not to have instability properties as the ones observed for Alex-net [28], because it applies contractive wavelet operators which are stable to deformations. However, deep neural networks with supervised training provide a clear improvement of average classification accuracy, compared to unsupervised learning and to this roto-translation scattering transform. This may indicate that they capture refined but important geometric image properties. Understanding the nature of these properties is an open challenge to further improve the performances of scattering representations.

Acknowledgments

This work is funded by the ERC grant InvariantClass 320959 and via a grant for Phd Students of the Conseil régional d’Île-de-France (RDM-IdF).

References

- [1] L. Bo, X. Ren, and D. Fox. Multipath Sparse Coding Using Hierarchical Matching Pursuit. In *CVPR*, pages 660–667. IEEE, 2013. 7
- [2] Y.-L. Boureau, N. L. Roux, F. Bach, J. Ponce, and Y. LeCun. Ask the locals: Multi-way local pooling for image recognition. In D. N. Metaxas, L. Quan, A. Sanfeliu, and L. J. V. Gool, editors, *ICCV*, pages 2651–2658. IEEE, 2011. 7
- [3] J. Bruna. Signal and Texture Recovery from Scattering Representations. 2014. 2, 5, 7
- [4] J. Bruna and S. Mallat. Invariant Scattering Convolution Networks. *IEEE Trans. Pattern Anal. Mach. Intell.*, 35(8):1872–1886, 2013. 1, 3, 4, 7
- [5] N. Dalal and B. Triggs. Histograms of oriented gradients for human detection. In *Computer Vision and Pattern Recognition, 2005. CVPR 2005. IEEE Computer Society Conference on*, volume 1, pages 886–893. IEEE, 2005. 1
- [6] R. B. Girshick, J. Donahue, T. Darrell, and J. Malik. Rich feature hierarchies for accurate object detection and semantic segmentation. *CoRR*, abs/1311.2524, 2013. 1, 8
- [7] K. He, X. Zhang, S. Ren, and J. Sun. Spatial pyramid pooling in deep convolutional networks for visual recognition. In *Computer Vision—ECCV 2014*, pages 346–361. Springer, 2014. 7
- [8] Y. Jia, C. Huang, and T. Darrell. Beyond spatial pyramids: Receptive field learning for pooled image features. In *CVPR*, pages 3370–3377. IEEE, 2012. 7, 8
- [9] A. Krizhevsky, I. Sutskever, and G. E. Hinton. ImageNet Classification with Deep Convolutional Neural Networks. In P. L. Bartlett, F. C. N. Pereira, C. J. C. Burges, L. Bottou, and

- K. Q. Weinberger, editors, *NIPS*, pages 1106–1114, 2012. [1](#), [2](#)
- [10] S. Lazebnik, C. Schmid, and J. Ponce. Beyond Bags of Features: Spatial Pyramid Matching for Recognizing Natural Scene Categories. In *CVPR (2)*, pages 2169–2178. IEEE Computer Society, 2006. [1](#), [7](#)
- [11] Q. V. Le, M. Ranzato, R. Monga, M. Devin, G. Corrado, K. Chen, J. Dean, and A. Y. Ng. Building high-level features using large scale unsupervised learning. In *ICML*. icml.cc / Omnipress, 2012. [1](#)
- [12] Y. Lecun, B. Boser, J. S. Denker, D. Henderson, R. E. Howard, W. Hubbard, and L. D. Jackel. Back-Propagation Applied to Handwritten Zip Code Recognition. *Neural Computation*, 1(4):541–551, 1989. [2](#)
- [13] Y. LeCun, K. Kavukcuoglu, and C. Farabet. Convolutional networks and applications in vision. In *ISCAS*, pages 253–256. IEEE, 2010. [2](#), [7](#)
- [14] C.-Y. Lee, S. Xie, P. Gallagher, Z. Zhang, and Z. Tu. Deeply-Supervised Nets. *arXiv preprint arXiv:1409.5185*, 2014. [1](#), [7](#), [8](#)
- [15] H. Lee, R. B. Grosse, R. Ranganath, and A. Y. Ng. Convolutional deep belief networks for scalable unsupervised learning of hierarchical representations. In A. P. Danyluk, L. Bottou, and M. L. Littman, editors, *ICML*, volume 382 of *ACM International Conference Proceeding Series*, page 77. ACM, 2009. [7](#)
- [16] T.-H. Lin and H. EDU. Stable and Efficient Representation Learning with Nonnegativity Constraints. [7](#), [8](#)
- [17] D. Lowe. Distinctive image features from scale-invariant key-points. *Intl. Journal of Computer Vision*, 60:91–110, 2004. [1](#), [5](#)
- [18] M. Malinowski and M. Fritz. Learning smooth pooling regions for visual recognition. In *the British Machine Vision Conference*, 2013. [7](#)
- [19] S. Mallat. *A Wavelet Tour of Signal Processing*. San Diego : Academic Press, 1999. [3](#)
- [20] S. Mallat. Group Invariant Scattering. *CoRR*, abs/1101.2286, 2011. [1](#), [2](#), [3](#), [5](#), [8](#)
- [21] S. McCann and D. G. Lowe. Spatially Local Coding for Object Recognition. In K. M. Lee, Y. Matsushita, J. M. Rehg, and Z. Hu, editors, *ACCV (1)*, volume 7724 of *Lecture Notes in Computer Science*, pages 204–217. Springer, 2012. [7](#)
- [22] R. Rosipal and N. Krämer. Overview and Recent Advances in Partial Least Squares. In C. Saunders, M. Grobelnik, S. R. Gunn, and J. Shawe-Taylor, editors, *SLSFS*, volume 3940 of *Lecture Notes in Computer Science*, pages 34–51. Springer, 2005. [5](#), [6](#)
- [23] A. M. Saxe, P. W. Koh, Z. Chen, M. Bhand, B. Suresh, and A. Y. Ng. On Random Weights and Unsupervised Feature Learning. In L. Getoor and T. Scheffer, editors, *ICML*, pages 1089–1096. Omnipress, 2011. [2](#), [7](#)
- [24] W. R. Schwartz, A. Kembhavi, D. Harwood, and L. S. Davis. Human detection using partial least squares analysis. In *ICCV*, pages 24–31. IEEE, 2009. [5](#)
- [25] L. Sifre and S. Mallat. Rotation, Scaling and Deformation Invariant Scattering for Texture Discrimination. In *CVPR*, pages 1233–1240. IEEE, 2013. [1](#), [3](#), [4](#)
- [26] J. Sivic, B. C. Russell, A. A. Efros, A. Zisserman, and W. T. Freeman. Discovering objects and their location in images. volume 1, pages 370–377, 2005. [1](#)
- [27] K. Sohn and H. Lee. Learning Invariant Representations with Local Transformations. In *ICML*. icml.cc / Omnipress, 2012. [7](#)
- [28] C. Szegedy, W. Zaremba, I. Sutskever, J. Bruna, D. Erhan, I. J. Goodfellow, and R. Fergus. Intriguing properties of neural networks. *CoRR*, abs/1312.6199, 2013. [2](#), [5](#), [8](#)
- [29] P. Vincent, H. Larochelle, Y. Bengio, and P.-A. Manzagol. Extracting and composing robust features with denoising autoencoders. In W. W. Cohen, A. McCallum, and S. T. Roweis, editors, *ICML*, volume 307 of *ACM International Conference Proceeding Series*, pages 1096–1103. ACM, 2008. [2](#)
- [30] M. D. Zeiler and R. Fergus. Visualizing and Understanding Convolutional Networks. *CoRR*, abs/1311.2901, 2013. [1](#), [7](#)
- [31] H. Zhang, S. Kiranyaz, and M. Gabbouj. Cardinal Sparse Partial Least Square Feature Selection And Its Application In Face Recognition. [5](#)